Journal of Electrical and Computer Engineering Innovations
(JECEI)
Journal homepage: http://www.jecei.sru.ac.ir

Research paper

Robust Fuzzy Control of Uncertain Two-axis Inertially Stabilized Platforms Using a Disturbance Observer: A Backstepping-based Adaptive Control Approach

M. Ghalehnoie [*]***, A. Azhdari, J. Keighobadi***

Faculty of Electrical Engineering, Shahrood University of Technology, Shahrood, Iran.

Article Info

Article History:
Received 08 May 2024
Reviewed 27 June 2024
Revised 30 July 2024
Accepted 09 August 2024

Keywords:
Inertially stabilized platform
Backstepping control
Disturbance observer
Fuzzy approximation
Model-free control

[*]Corresponding Author's Email Address:
ghalehnoie@shahroodut.ac.ir

Abstract

Background and Objectives: The two-axis inertially stabilized platforms (ISPs) face various challenges such as system nonlinearity, parameter fluctuations, and disturbances which makes the design process more complex. To address these challenges effectively, the main objective of this paper is to realize the stabilization of ISPs by presenting a new robust model-free control scheme.

Methods: In this study, a robust adaptive fuzzy control approach is proposed for two-axis ISPs. The proposed approach leverages the backstepping method as its foundational design mechanism, employing fuzzy systems to approximate unknown terms within the control framework. Furthermore, the control architecture incorporates a model-free disturbance observer, enhancing the system's robustness and performance. Additionally, novel adaptive rules are devised, and the uniform ultimate boundedness stability of the closed-loop system is rigorously validated using the Lyapunov theorem.

Results: Using MATLAB/Simulink software, simulation results are obtained for the proposed control system and its performance is assessed in comparison with related research works across two scenarios. In the first scenario, where both the desired and initial attitude angles are set to zero, the proposed method demonstrates a substantial mean squared error (MSE) reduction: 96.2% for pitch and 86.7% for yaw compared to the backstepping method, and reductions of 75% for pitch and 33.3% for yaw compared to the backstepping sliding mode control. In the second scenario, which involves a 10-degree step input, similar improvements are observed alongside superior performance in terms of reduced overshoot and settling time. Specifically, the proposed method achieves a settling time for the pitch gimbal 56.6% faster than the backstepping method and 58% faster for the yaw gimbal. Moreover, the overshoot for the pitch angle is reduced by 53.5% compared to backstepping and 35.5% compared to backstepping sliding mode control, while for the yaw angle, reductions of 43.6% and 37.6% are achieved, respectively.

Conclusion: Through comprehensive simulation studies, the efficacy of the proposed algorithm is demonstrated, showcasing its superior performance compared to conventional control methods. Specifically, the proposed method exhibits notable improvements in reducing maximum deviation from desired angles, mean squared errors, settling time, and overshoot, outperforming both backstepping and backstepping sliding mode control methods.

Introduction

Unmanned aerial inspection systems face challenges in maintaining optical imaging sensors' direction due to angular disturbances from vehicle motion, wind, and measurement errors. To tackle this, inertially stabilized platforms (ISPs) with gimbal assemblies are commonly employed [1]-[4]. However, the complex dynamics of

multi-axis ISPs, including strong nonlinearity and various uncertainties, make stabilization challenging [5]-[10].

The PID controller stands out as a popular choice in practical applications for its simple implementation. However, its derivative term can exacerbate high-frequency disturbances, leading to rapid saturation of the controller output. To address this, modern modifications are used to automatically adjust control coefficients in different operating conditions, such as using the fuzzy approach in ISPs [11], [12]. Yet, increasing the number of fuzzy partitions complicates controller design and implementation. Thus, the fuzzy controller structure is often kept simple, impacting the PID controller's performance in ISP environments with uncertainties and disturbances.

Researchers employ robust control strategies to tackle uncertainties in nonlinear systems. For example, in [13], authors investigate magnetically suspended gimbals and develop an H_∞ method. Also, [14] proposes a mixed sensitivity H_∞ controller for ISPs, aiming to strike a balance between robustness and performance. These static strategies assume bounded variables, and their complexity increases with uncertainty levels, impacting system efficiency.

Besides, sliding mode control (SMC) methods are favored for severely nonlinear systems like ISPs due to their robustness against uncertainty [15]. As an example, [5] introduces a standard SMC to counter disturbances, while [4] proposes the super-twisting method to address chattering issues. Integral sliding mode control (ISMC), suggested in [16] and [17], further mitigates nonlinear disturbances and uncertainties in ISPs. However, the growing complexity of dynamic models and uncertainties diminishes SMC effectiveness. So, some combine SMC with the backstepping approach, as seen in [18]-[22]. Nevertheless, designing a robust backstepping-based controller for ISPs remains a challenge. For instance, [23] introduces an innovative adaptive neural network model integrated with backstepping control to address the difficulties posed by unknown disturbances and dynamics in nonlinear three-degree-of-freedom (3-DOF) ISPs. ISPs can feature either two or three DOF, each configuration offering distinct benefits. A 2-DOF ISP generally consists of a two-axis gimbal assembly, providing stabilization over two axes such as azimuth and elevation [24]. Conversely, a 3-DOF ISP comprises a three-axis gimbal, enabling stabilization over three axes, thus facilitating more complex motion compensation and greater flexibility in target tracking. The additional degree of freedom in a 3-DOF ISP allows for more comprehensive control over the line of sight and offers enhanced disturbance rejection capabilities, making it suitable for high-accuracy applications [25], [26]. In contrast, a 2-DOF ISP is often more cost-effective and simpler to implement due to its reduced complexity and fewer moving parts [27]. However, it may face limitations in compensating for certain disturbances and body motions, especially in scenarios involving large payloads or significant external disturbances.

To the best of author's knowledge, the most effective strategy for mitigating lumped uncertainties involves using disturbance observers and rejection methods alongside well-designed controllers [23], [28]-[30]. For instance, [5] introduces continuous terminal sliding mode control with high-order sliding mode observers for estimating state variables and uncertainties, while [17] combines terminal sliding mode control with extended state observers in ISPs. Additionally, [31] presents a model predictive control method using a discrete-time disturbance observer, and [4] proposes continuous SMC with finite time disturbance observers. Besides, [32] presents an adaptive SMC algorithm for ISPs using disturbance observers. Also, [33] employs an Uncertainty and Disturbance Estimator (UDE) to estimate the composite disturbance and enhance the robustness of a Feedback Linearization-based controller designed for a 3-DOF known nominal ISP system. These model-based methods enhance control performance by estimating disturbances, although model's accuracy significantly impact their efficacy.

In contrast to model-based disturbance observers, whose performance depends on the system model's accuracy, model-free disturbance observers estimate lumped uncertainties using techniques such as neural networks. For example, [8] proposes an RBFNN-based adaptive disturbance control method for effective uncertainty estimation. However, using a linear system model significantly increases uncertainty levels and impacts observer performance.

Another drawback is the neglect of rate of change in disturbances or estimation error. As well, [22] and [34] combines a backstepping sliding mode control with an adaptive radial basis function neural network estimator to address parametric uncertainties, friction, mass imbalance, and uncertain disturbances. They believe the sampling estimation period can be small in comparison to these variations.

The above studies show that the dynamic model of ISPs is so complex and highly nonlinear that accurate mathematical modeling of all physical aspects is impossible. On the other hand, increasing the complexity of the model makes the control design and its implementation challenging. Therefore, researchers use models that include a variety of uncertainty resources, including parametric and structural uncertainties as well as internal and external disturbances. Controllers that use inaccurate dynamics or do not consider existing

disturbances or those that approximate the uncertainties based on the inaccurate model are doomed to failure in practice. However, the dynamical structure of ISPs is in a particular class of nonlinear systems in which the benefits of backstepping can be used. Despite the advantages of backstepping control, not using precise dynamics and not paying attention to the lumped uncertainties leads to irreparable consequences. Inspired by [35], [36], to tackle these issues, fuzzy approximators and disturbance observers can be coupled to estimate unknown dynamics and disturbances, respectively.

Inspired by the related literature, the main difficulties can be stated as follows:

- The existence of time-varying disturbances and highly nonlinearities in the system model makes it challenging to design a learning-based robust adaptive controller to deal with both of them.
- Considering the system dynamics as unknown terms brings us closer to the real-world applications. Thus, how to design a disturbance observer on the basis of unknown system dynamics is an important issue.
- Achieving robust stability of the overall system in the presence of various uncertainties is a serious issue.

So, this paper introduces a fuzzy disturbance observer-based backstepping control to track desired trajectories amidst uncertainties. It employs a nonlinear model-free disturbance observer to approximate time-varying disturbances, uncertainties, and fuzzy errors. This method enhances system performance by sharing information between the fuzzy approximator and disturbance observer. Besides, stability is verified via recursive Lyapunov-based analysis.

pitch frame (p) with the coordinate system $\{x_p, y_p, z_p\}$,

As clearly observed in Table 1, compared with the current relevant studies, the primary contributions of the suggested controller are as follows:

i) For the ISP systems, this study is the first attempt to handle the various uncertainties, including time-varying disturbances and highly nonlinearities, by employing an adaptive fuzzy-based disturbance observer.

ii) Integrating the fuzzy learning algorithm with the model-free disturbance observer improves the system performance while the system information is not required during the process.

iii) The design mechanism is based on the backstepping method, where the overall system's stability is proven by compensating for the error of each subsystem for the ISP systems. In other words, if an adverse result occurs, it is easier to find its origination.

The rest of this paper is arranged as follows. Section 2 discusses the modeling of a two-axis ISP system, concluding that the resulting state space has a low triangular structure and contains structural and parametric uncertainty. Section 3 uses this structure to develop a controller based on the backstepping approach. However, to improve performance, the nonlinear dynamics of the model are assumed to be unknown and are identified by a fuzzy approximation. Also, a model-free disturbance observer estimates the disturbances and the fuzzy approximation errors. The control signal exploits the approximated dynamics and disturbances, and the stability conditions are expressed. Section 4 presents the simulation results, followed by Section 5's conclusions.

Table 1: Comparative analysis of implementation strategies for ISP systems

Reference	Model Linearity	Model-based/free	DOB-based	Disturbance Type
[3]	nonlinear	model-free	No	time-invariant and bounded
[4]	nonlinear	model-based	No	time-varying
[5], [19]	linear	model-based	Yes	not determined
[16], [29], [31]	linear	model-based	yes	time-varying
[8]	linear	model-free	yes	time-invariant and bounded
[17], [33], [37], [38]	nonlinear	model-based	yes	time-invariant and bounded
[6], [22], [34]	nonlinear	model-free	yes	time-invariant and bounded
proposed approach	nonlinear	model-free	yes	time-varying

Modeling of Two-Axis ISPs

Fig. 1 illustrates a typical two-axis ISP architecture, comprising three frames crucial for coupling analysis: the yaw frame (a) with $\{x_a, y_a, z_a\}$, and the base frame (b) with $\{x_b, y_b, z_b\}$. Notably, a two-axis gyro is incorporated for line-of-sight control, influenced by the

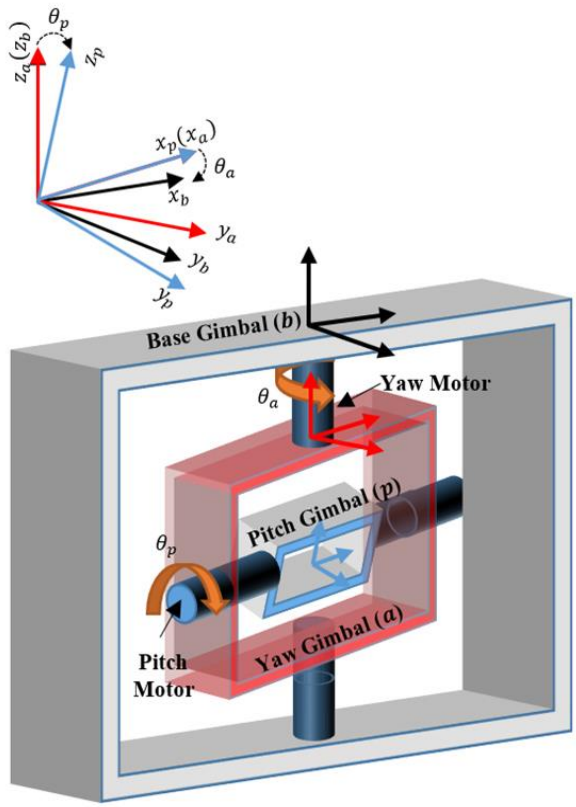

Fig. 1: A typical configuration diagram for two-gimbal ISPs and the related coordinate frames.

movements of the pitch and yaw gimbals.

Encoders installed on the pitch and yaw gimbals measure their angular positions. The relative angular displacement between the base plate and the yaw gimbal is represented by θ_a, while θ_p denotes the relative angular displacement between the yaw and pitch gimbals. Moreover, the angular rates between the gimbal coordinates are denoted as $\dot{\theta}_a$ and $\dot{\theta}_p$. By employing Euler transformation matrices, namely C_b^a and C_a^p, which pertain to rotations about the x-axis and the z-axis respectively, the angular rates of gimbals are specified as,

$$\begin{aligned}\omega_{na}^{a} &= \left[\omega_{nax}^{a}, \omega_{nay}^{a}, \omega_{naz}^{a}\right]^T = C_b^a \omega_{nb}^{b} + \left[0, 0, \dot{\theta}_a\right]^T \\ &= \begin{bmatrix} \omega_{nbx}^{b}\cos\theta_a + \omega_{nby}^{b}\sin\theta_a \\ -\omega_{nbx}^{b}\sin\theta_a + \omega_{nby}^{b}\cos\theta_a \\ \omega_{nbz}^{b} + \dot{\theta}_a \end{bmatrix},\end{aligned} \tag{1}$$

$$\begin{aligned}\omega_{np}^{p} &= \left[\omega_{npx}^{p}, \omega_{npy}^{p}, \omega_{npz}^{p}\right]^T = C_a^p \omega_{na}^{a} + \left[\dot{\theta}_p, 0, 0\right]^T \\ &= \begin{bmatrix} \omega_{nax}^{a} + \dot{\theta}_p \\ \omega_{nay}^{a}\cos\theta_p + \omega_{naz}^{a}\sin\theta_p \\ -\omega_{nay}^{a}\sin\theta_p + \omega_{naz}^{a}\cos\theta_p \end{bmatrix}.\end{aligned} \tag{2}$$

Since the base frame is tied to the helicopter, $\omega_{nb}^{b} = \left[\omega_{nbx}^{b}, \omega_{nby}^{b}, \omega_{nbz}^{b}\right]^T$ is the helicopter's angular velocity.

A. Dynamics of Gimbals

If the gimbals are treated as rigid bodies, their motion equations can be derived using the Newton–Euler theory.

The total external torques are expressed as follows,

$$T_a = \dot{H}_a + \omega_{na}^{a} \times H_a, \qquad T_P = \dot{H}_p + \omega_{np}^{p} \times H_p, \tag{3}$$

where $T_a = \left[T_{ax}, T_{ay}, T_{az}\right]^T$ denotes the total external torque about the yaw gimbal, $T_p = \left[T_{px}, T_{py}, T_{pz}\right]^T$ represents the total external torque applied to the pitch gimbal, and H_a and H_p signify the total angular momentum of the gimbals. Assuming symmetry for each gimbal with respect to its coordinate and neglecting inertia products, the moment of inertia for the two gimbals is defined as,

$$\begin{aligned} J_a &= diag\left(J_{ax}, J_{ay}, J_{az}\right), \\ J_p &= diag\left(J_{px}, J_{py}, J_{pz}\right) \end{aligned} \tag{4}$$

Here, it is assumed that the gimbals have balanced masses. By substituting the angular momentums, angular rates, and total external torques about the yaw gimbal's x-axis and the pitch gimbal's z-axis into (3), the dynamic model of the gimbals is obtained. The pitch gimbal's angular momentum is,

$$H_p = J_p \omega_{np}^{p}. \tag{5}$$

Substituting (5) in (3) leads to the pitch gimbal's angular momentum about the x-axis,

$$T_{px} = J_{px}\, \dot{\omega}_{npx}^{p} + \left(J_{pz} - J_{py}\right) \omega_{npy}^{p}\, \omega_{npz}^{p}. \tag{6}$$

Due to the connection between the pitch and yaw gimbals, the yaw gimbal's inertial angular momentum is,

$$H_a = C_p^a\, H_p + J_a\, \omega_{na}^{a} \tag{7}$$

Thus, by utilizing (3), the projection of the resultant angular momentum along the yaw gimbal's z-axis can be derived as,

$$\begin{aligned} T_{az} = &\left(J_{az}\, \omega_{naz}^{a}\right. \\ &+ \left(J_{py}\cos^2\theta_p + J_{pz}\sin^2\theta_p\right) \omega_{naz}^{a}\Big)' \\ &+ \Big(\left(J_{py} - J_{pz}\right)\cos\theta_p \sin\theta_p\, \omega_{nay}^{a}\Big)' \\ &+ \left(J_{ay} + J_{py}\, \cos^2\theta_p\right. \\ &\left. + J_{pz}\, \sin^2\theta_p\right)\omega_{nax}^{a}\, \omega_{nay}^{a} \\ &- J_{ax}\omega_{nax}^{a}\, \omega_{nay}^{a} - J_{px}\, \omega_{npx}^{p}\, \omega_{nay}^{a} \\ &+ \left(J_{py} - J_{pz}\right)\, \cos\theta_p \sin\theta_p\, \omega_{naz}^{a}\, \omega_{nax}^{a} \end{aligned} \tag{8}$$

where the prime operator signifies the time derivative. To finalize the development of a dynamic model for a two-axis ISP, the subsequent section elaborates on formulating a dynamical model for a DC motor linked to

each gimbal.

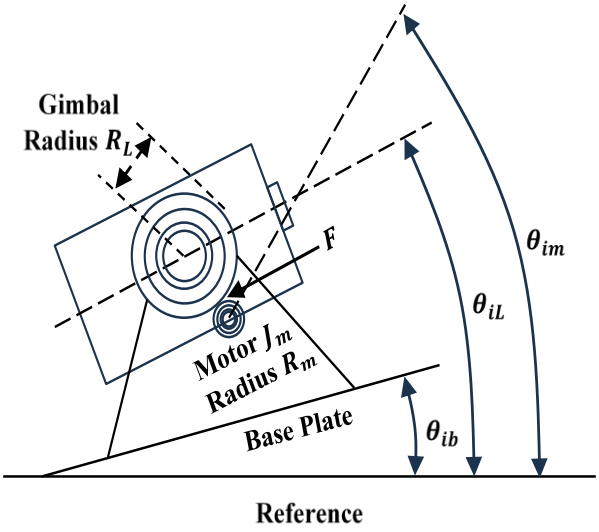

Fig. 2: A single gimbal gear-drive system [3].

B. Dynamical Model of Motor

The high imaging loads necessitate the use of a DC motor with a gearbox, as depicted in Fig. 2, instead of a direct-driven torque motor to ensure stable control [3]. In Fig. 2, F signifies the interacting force between the motor gear and the gimbal gear, with R_m and R_L denoting their respective radii, and where $L \in \{p, a\}$ represents the pitch and yaw gimbals. Furthermore, $N = R_L/r$ stands for the gear ratio.

In a gear-driven system, the torque applied to the gimbal is given by,

$$T_L = R_L F + T_{dL} \tag{9}$$

while the motor's angular acceleration is described by,

$$\ddot{\theta}_{nm} = (K_t\, i_m - rF + T_{dm})/J_m \tag{10}$$

where θ_{nm} is the attitude of the gimbal's motor, K_t denotes the torque constant, and i_m stands for the motor's armature current. Also, external torque perturbations affecting the gimbal and the motor are represented by T_{dL} and T_{dm}, respectively, predominantly reflecting the influences of mass imbalance, bearing friction, and gearing friction.

Considering the electrical characteristics of a DC motor's equivalent armature circuit, the armature voltage u is defined as,

$$u_L = K_e\, \dot{\theta}_{m/b} + R_m\, i_m + L_m\, di_m/dt \tag{11}$$

Here, L_m and R_m signify the motor's inductance and resistance, respectively, while K_e stands for the back electromotive force constant. Moreover, $\theta_{m/b}$ represents the motor's motion relative to the base plate. Additionally, the kinematic relations of the system are as follows,

$$\theta_{nL} = \theta_{L/b} + \theta_{nb} \tag{12}$$

$$\theta_{nm} = \theta_{m/b} + \theta_{nb} \tag{13}$$

$$\theta_{m/b} = N\, \theta_{L/b} \tag{14}$$

In these equations, θ_{nL} and θ_{nb} denote the attitudes of the gimbal and the base with regard to inertial space, respectively, while $\theta_{L/b}$ represents the gimbal's motion relative to the base plate.

By disregarding the negligible value of motor inductance and utilizing (11) to (14), we obtain,

$$T_m = K_t i_m = K_t/R_m \left(u_L - K_e\left(\dot{\theta}_{nm} - \dot{\theta}_{nb}\right)\right) \tag{15}$$

Also, by substituting (15) into (10) and subsequently utilizing (9), T_L is derived as follows,

$$\begin{aligned} T_L = {} & K_t/R_m \left(u_L - K_e\left(\dot{\theta}_{nm} - \dot{\theta}_{nb}\right)\right) \\ & - N^2\, J_m\, \ddot{\theta}_{nL} + (N\, T_{dm} + T_{dL}) \\ & + N(N-1)\, J_m\, \dot{\theta}_{nb} \end{aligned} \tag{16}$$

In (16), accounting for the yaw gimbal, the subscript L corresponds to a, thus $\theta_{nb} = \theta^a_{nbz}$, $\theta_{nL} = \theta^a_{na}$, and $T_L = T_{az}$. Similarly, for the pitch gimbal, we have $\theta_{nb} = \theta^p_{nbz}$, $\theta_{nL} = \theta^p_{np}$, and $T_L = T_{px}$.

Finally, considering (6), (8), and (16), one can conclude the dynamic model of a two-axis ISP as follows,

$$\dot{\omega}^p_{npx} = f_1(t) + b_1 u_1 + d_1 \tag{17}$$

$$\dot{\omega}^a_{naz} = f_2(t) + b_2 u_2 + d_2 \tag{18}$$

in which,

$$u_1 = u_p, \qquad u_2 = u_a \tag{19}$$

$$\begin{aligned} b_1 &= NK_t/\left(R_m\left(J_{px} + N^2\, J_m\right)\right) \\ b_2 &= \frac{NK_t \cos\theta_p}{R_m\left(J_{az} + N^2 J_m + J_{pz}\cos^2\theta_p\right)} \end{aligned} \tag{20}$$

$$\begin{aligned} f_1(t) = {} & \frac{K_t\, K_e\, N^2\, \left(\omega^p_{nax} - \omega^p_{npx}\right)}{\left(J_{px} + N^2\, J_m\right)R_m} \\ & + \frac{N\,(N-1)\, R_m\, J_m\, \dot{\omega}^p_{nax}}{\left(J_{px} + N^2\, J_m\right)R_m} \\ & - \frac{\left(J_{pz} - J_{py}\right)\omega^p_{npy}\omega^p_{npz}}{J_{px} + N^2\, J_m} \end{aligned} \tag{21}$$

$$
\begin{aligned}
& f_2(t) \\
&= \frac{\cos\theta_p\,\omega_{nay}^a\left(\omega_{npx}^p J_{px} - \omega_{nax}^a\left(J_{ay} - J_{ax}\right)\right)}{J_{az} + N^2 J_m + J_{pz}\cos^2\theta_p} \\
&+ \frac{N^2 K_t K_e \cos\theta_p\,(\omega_{nbz}^a - \omega_{naz}^a)}{R_m\left(J_{az} + N^2 J_m + J_{pz}\cos^2\theta_p\right)} \\
&+ \frac{N(N-1)\cos\theta_p\,R_m J_m\,\dot{\omega}_{nbz}^a}{R_m\left(J_{az} + N^2 J_m + J_{pz}\cos^2\theta_p\right)} \\
&+ \frac{J_{pz}\,\omega_{npz}^p \sin 2\theta_p\left(\dot{\theta}_p + \omega_{nax}^a\right)}{2\left(J_{az} + N^2 J_m + J_{pz}\cos^2\theta_p\right)} \\
&- \frac{J_{py}\,\omega_{npy}^p\,\omega_{nax}^a\,\cos^2\theta_p}{J_{az} + N^2 J_m + J_{pz}\cos^2\theta_p} \\
&- \frac{\Psi(t)}{J_{az} + N^2 J_m + J_{pz}\cos^2\theta_p}
\end{aligned}
\tag{22}
$$

$$
\begin{aligned}
\Psi(t) = {} & \cos\theta_p\,\left(J_{py}\,\omega_{npy}^p \sin\theta_p\right)' \\
& + \left(J_{az} + J_{py}\cos^2\theta_p + J_{pz}\sin^2\theta_p\right. \\
& \left. + N^2 J_m\right)\left(\omega_{naz}^a\,\sin\theta_p\,\dot{\theta}_p\right. \\
& \left. + \left(\omega_{nay}^a\,\sin\theta_p\right)'\right)
\end{aligned}
$$

$$
d_1 = \left(N\,T_{dm} + T_{dp} + \Lambda_1\right)/\left(J_{px} + N^2 J_m\right) \tag{23}
$$

$$
d_2 = \frac{N T_{dm} + T_{da} + \Lambda_2}{J_{az} + N^2 J_m + J_{pz}\cos^2\theta_p}\cos\theta_p \tag{24}
$$

where other angular velocities can be calculated using (1) and (2) in terms of the helicopter's angular velocity ω_{nb}^b.

In ISP systems, the moments of inertia (i.e., J_a and J_p) are subject to estimation due to imprecise knowledge. These estimation errors, along with other parametric and structural uncertainties, are accounted for in dynamic equations (17)-(24) by Λ_1 and Λ_2. However, considering all uncertainties in system dynamics, particularly in f_1 and f_2, which are highly complex and nonlinear, can lead to excessive uncertainty levels and consequently poor system performance. Therefore, in the following, only f_1 and f_2 are treated as unknown and approximated using a Takagi-Sugeno fuzzy approximator. In addition, the fuzzy estimate errors in each subsystem, along with terms d_1 and d_2, are regarded as a lumped disturbance. To approximate this lumped disturbance, disturbance observers utilize the approximated nonlinear terms f_1 and f_2.

Hence, by defining the state variables $x_1 = \theta_{nx}^p$, $x_2 = \dot{\theta}_{nx}^p = \omega_{npx}^p$, $x_3 = \theta_{nz}^a$, and $x_4 = \dot{\theta}_{nz}^a = \omega_{naz}^a$, the ISP system's state-space model is obtained as,

$$\dot{x}_1 = x_2 \tag{25}$$

$$\dot{x}_2 = f_1 + b_1 u_1 + d_1 \tag{26}$$

$$\dot{x}_3 = x_4 \tag{27}$$

$$\dot{x}_4 = f_2 + b_2 u_2 + d_2 \tag{28}$$

here, the nonlinear terms f_1 and f_2 are generally unknown, with all parametric and structural uncertainties encapsulated in the d_1 and d_2. This model comprises two subsystems with a low-triangular structure, enabling the utilization of backstepping control in its controller design.

Main Results

This section aims to design an adaptive fuzzy backstepping controller equipped with a model-free disturbance observer for the system (25)-(28). Following the backstepping method, the proposed approach involves four steps. As mentioned, to increase the efficiency of the designed controller, $f_i,\ i \in \{1,2\}$ is considered unknown, which is approximated by a Sugeno-type fuzzy logic system,

$$R^k: IF\ x_1 is\ F_{i1}^k\ and\ \dots and\ x_n is\ F_{in}^k\ Then\ \hat{f}_i = \Gamma_{ik}$$

where $x = (x_1, \dots, x_n)^T$ is the inputs of fuzzy system, $k = 1, 2, \dots, l$ is the rule number and l is the number of rules, F_{i1}^k is the fuzzy set with the membership function $\mu_{F_{ij}^k}(x_j)$, and Γ_{ik} is a constant value. Using singleton fuzzifier, product inference and weighted average defuzzification, we obtain [39],

$$\hat{f}_i = \Gamma_i^T \phi_i(x)$$

where $\phi_i(x) = [\phi_{i1}(x), \phi_{i2}(x), \dots, \phi_{il}(x)]^T$, and $\phi_{ik}(x) = \prod_{j=1}^n \mu_{F_{ij}^k}(x_j) / \sum_{m=1}^l \prod_{j=1}^n \mu_{F_{ij}^m}(x_j)$ is the membership function of the j^{th} rule's antecedent part. Besides, $\Gamma_i^T = [\Gamma_{i1}, \Gamma_{i2}, \dots, \Gamma_{il}]^T$ is the fuzzy weight vector. Considering the fuzzy approximation error ϵ_i,

$$f_i(x) = \Gamma_i^{*T} \phi_i(x) + \epsilon_i \tag{29}$$

where $\Gamma_i^* = [\Gamma_{i1}^*, \Gamma_{i2}^*, \dots, \Gamma_{il}^*]^T$is the optimal fuzzy weight vector. Since f_i and its corresponding optimal fuzzy weight vector Γ_i^* are unknown, their estimations is used in the control signals. In other words, $\hat{f}_i = \hat{\Gamma}_i^{*T} \phi_i$ is employed in the proposed control signals, in which $\hat{\Gamma}_i^*$ is the estimated fuzzy weight vector such that the error of the fuzzy weight vector $\tilde{\Gamma}_i = \Gamma_i^* - \hat{\Gamma}_i$ should converge to zero ultimately. However, the fuzzy approximation error ϵ_i and the uncertainties $g_i d_i$ are considered lumped

disturbance $D_i = d_i + \epsilon_i$ which is observed using a disturbance observer $\widehat{D}_i$. This leads to enhancing the robust behavior of the control system. It is assumed that positive real scalars bound the lumped disturbance D_i and its variation. In other words, we assume $\dot{D}_i^T \dot{D}_i \leq \zeta_i^2$, where $\zeta_i > 0$ is a known positive real scalar. Here, the conservative assumption of zero variation is not considered. Furthermore, since the input membership functions $\phi_{ij}(x_i)$, $i \in \{1,2\}$ and $j \in \{1,2,\dots,l\}$ are known, it is clear that $\phi_i^T \phi_i \leq \eta_i^2$ where $\eta_i > 0$ is known. More details are given in the following.

Step 1) For the first subsystem (25) the tracking error is defined as,

$$\omega_1 = x_1 - x_1^d \tag{29}$$

in which x_1^d is the desired reference signal. We choose the first virtual control,

$$\beta_1 = -k_1\omega_1 + \dot{x}_1^d \tag{30}$$

where k_1 is a positive real constant. For the 2nd subsystem (26), the error surface $\omega_2 = x_2 - \beta_1$ is defined. Thus, the derivative of the tracking error ω_1 is as follows,

$$\dot{\omega}_1 = \dot{x}_1 - \dot{x}_1^d = x_2 - \dot{x}_1^d = \omega_2 + \beta_1 - \dot{x}_1^d \tag{31}$$

Substituting (30) into (31) yields,

$$\dot{\omega}_1 = -k_1\omega_1 + \omega_2 \tag{32}$$

Now, choosing the Lyapunov function $V_1 = \frac{1}{2}\omega_1^2$ and considering (32) leads us to,

$$\dot{V}_1 = -k_1\omega_1^2 + \omega_1\omega_2 \tag{33}$$

Step 2) The derivative of the 2nd subsystem's error surface is,

$$\dot{\omega}_2 = \dot{x}_2 - \dot{\beta}_1 = \Gamma_1^{*T}\phi_1 + b_1u_1 - \dot{\beta}_1 + D_1 \tag{34}$$

where $D_1 = d_1 + \epsilon_1$ is the lumped disturbance. Considering the control signal,

$$u_1 = \left(-\hat{\Gamma}_1^{\mathrm{T}}\phi_1 - k_2\omega_2 - \omega_1 + \dot{\beta}_1 - \widehat{D}_1\right)/b_1 \tag{35}$$

in which $k_2 > 0$ is a real scalar and $\widehat{D}_1$ is the lumped disturbance's estimation, and then substituting it into (34) gives,

$$\dot{\omega}_2 = \tilde{\Gamma}_1^T\phi_1 + \tilde{D}_1 - \omega_1 - k_2\omega_2 \tag{36}$$

In this step, the Lyapunov function is chosen as,

$$V_2 = V_1 + \frac{1}{2}\omega_2^2 + \frac{1}{2}\tilde{\Gamma}_1^T\gamma_1^{-1}\tilde{\Gamma}_1 + \frac{1}{2}\tilde{D}_1^2 \tag{37}$$

where $\gamma_1 > 0$ is the learning rate of adaptation mechanism. Hence, one can obtain,

$$\begin{aligned}\dot{V}_2 = &-k_1\omega_1^2 - k_2\omega_2^2 + \tilde{\Gamma}^T{}_1\left(\omega_2\phi_1 - \gamma_1^{-1}\dot{\hat{\Gamma}}_1\right)\\ &+ \tilde{D}_1\left(\omega_2 + \dot{D}_1 - \dot{\hat{D}}_1\right)\end{aligned} \tag{38}$$

Using the fuzzy approximation for f_1, we define the following model-free disturbance observer,

$$\begin{aligned}\widehat{D}_1 &= L_1(x_2 - \chi_2)\\ \dot{\chi}_2 &= \hat{\Gamma}_1^{\mathrm{T}}\phi_1 + b_1u_1 + \widehat{D}_1 - L_1^{-1}\omega_2\end{aligned} \tag{39}$$

in which L_1 is a positive real constant; and the derivative of $\widehat{D}_1$ is,

$$\dot{\hat{D}}_1 = L_1(\dot{x}_2 - \dot{\chi}_2) = L_1\left(\tilde{\Gamma}_1^T\phi_1 + \tilde{D}_1\right) + \omega_2 \tag{40}$$

Employing (40) in (38),

$$\begin{aligned}\dot{V}_2 = &-k_1\omega_1^2 - k_2\omega_2^2 + \tilde{\Gamma}_1^T\left(\omega_2\phi_1 - \gamma_1^{-1}\dot{\hat{\Gamma}}_1\right)\\ &+ \tilde{D}_1\left(\dot{D}_1 - L_1\left(\tilde{\Gamma}_1^T\phi_1 + \tilde{D}_1\right)\right)\end{aligned} \tag{41}$$

Now, we choose the first adaptation law,

$$\dot{\hat{\Gamma}}_1 = \gamma_1\left(\omega_2\phi_1 - \delta_1\hat{\Gamma}_1\right) \tag{42}$$

where $\delta_1 > 0$ is a real scalar. Using Young inequality, one can find,

$$\begin{aligned}\tilde{D}_1\dot{D}_1 &\leq \frac{1}{2}\tilde{D}_1^2 + \frac{1}{2}\zeta_1^2\\ -\tilde{D}_1\tilde{\Gamma}_1^T\phi_1 &\leq \frac{1}{2}\omega_1\tilde{D}_1^2\eta_1^2 + \frac{1}{2\omega_1}\tilde{\Gamma}_1^T\tilde{\Gamma}_1\\ \tilde{\Gamma}_1^T\hat{\Gamma}_1 &\leq -\frac{1}{2}\tilde{\Gamma}_1^T\tilde{\Gamma}_1 + \frac{1}{2}\|\Gamma_1^*\|^2\end{aligned} \tag{43}$$

in which $\omega_1 > 0$. Then, $\dot{V}_2$ is obtained as,

$$\begin{aligned}\dot{V}_2 \leq &-k_1\omega_1^2 - k_2\omega_2^2 - \left(\frac{\delta_1}{2} - \frac{L_1}{2\omega_1}\right)\tilde{\Gamma}_1^T\tilde{\Gamma}_1\\ &- \left(L_1 - \frac{L_1\omega_1}{2}\eta_1^2 - \frac{1}{2}\right)\tilde{D}_1^2\\ &+ \left(\frac{\delta_1}{2}\|\Gamma_1^*\|^2 + \frac{1}{2}\zeta_1^2\right)\end{aligned} \tag{44}$$

Step 3) Considering the desired trajectory x_3^d for the state variable x_3 and define the error surface $\omega_3 = x_3 - x_3^d$, we have,

$$\dot{\omega}_3 = \dot{x}_3 - \dot{x}_3^d = x_4 - \dot{x}_3^d = \omega_4 + \beta_2 - \dot{x}_3^d \tag{45}$$

Another virtual control law is constructed as $\beta_2 = -k_3\omega_3 + \dot{x}_3^d$, where k_3 is a positive constant. This is then substituted in (17), resulting in,

$$\dot{\omega}_3 = -k_3\omega_3 + \omega_4 \tag{46}$$

Considering the Lyapunov function $V_3 = V_2 + \frac{1}{2}\omega_3^2$ as well as (44) and (46), one can obtain,

$$\begin{aligned}\dot{V}_3 \leq &-k_1\omega_1^2 - k_2\omega_2^2 - k_3\omega_3^2 + \omega_3\omega_4\\ &- \left(\frac{\delta_1}{2} - \frac{L_1}{2\omega_1}\right)\tilde{\Gamma}_1{}^T\tilde{\Gamma}_1\\ &- \left(L_1 - \frac{L_1\omega_1}{2}\eta_1^2 - \frac{1}{2}\right)\tilde{D}_1^2\\ &+ \left(\frac{\delta_1}{2}\|\Gamma_1^*\|^2 + \frac{1}{2}\zeta_1^2\right)\end{aligned} \tag{47}$$

Step 4) The error surface for the last subsystem (28) is defined as $\omega_4 = x_4 - \beta_2$. Hence, its derivative is,

$$\dot{\omega}_4 = \Gamma_2^{*T}\phi_2 + b_2 u_2 + D_2 - \dot{\beta}_2 \tag{48}$$

in which $D_2 = \epsilon_2 + d_2$ is the total disturbance include the fuzzy approximation error ϵ_2 for the term f_2 and the other modeling uncertainties d_2. The second control law is proposed as,

$$u_2 = \left(-\hat{\Gamma}_2^{\mathrm{T}}\phi_2 - k_4\omega_4 - \omega_3 + \dot{\beta}_2 - \hat{D}_2\right)/b_2 \tag{49}$$

where $k_4 > 0$ and $\hat{D}_2$ is the estimation of D_2. Substituting (49) into (48) results in,

$$\dot{\omega}_4 = \hat{\Gamma}_2^{\mathrm{T}}\phi_2 + \tilde{D}_2 - k_4\omega_4 - \omega_3 \tag{50}$$

The final Lyapunov function is chosen as,

$$V_4 = V_3 + \frac{1}{2}\omega_4^2 + \frac{1}{2}\tilde{\Gamma}_2^T\gamma_2^{-1}\tilde{\Gamma}_2 + \frac{1}{2}\tilde{D}_2^2 \tag{51}$$

where $\gamma_2 > 0$. The derivative of V_4 can be obtained as,

$$\begin{aligned}\dot{V}_4 \le\ & -k_1\omega_1^2 - k_2\omega_2^2 - k_3\omega_3^2 - k_4\omega_4^2 \\ & + \tilde{\Gamma}_2^T\left(\omega_4\phi_2 - \gamma_2^{-1}\dot{\hat{\Gamma}}_2\right) \\ & + \tilde{D}_2\left(\omega_4 + \dot{D}_2 - \dot{\hat{D}}_2\right) - \left(\frac{\delta_1}{2} - \frac{L_1}{2\omega_1}\right)\tilde{\Gamma}_1^{\ T}\tilde{\Gamma}_1 \\ & - \left(L_1 - \frac{L_1\omega_1}{2}\eta_1^2 - \frac{1}{2}\right)\tilde{D}_1^2 \\ & + \left(\frac{\delta_1}{2}\|\Gamma_1^*\|^2 + \frac{1}{2}\zeta_1^2\right)\end{aligned} \tag{52}$$

Similar to the step 2, the following model-free disturbance observer is designed,

$$\begin{aligned}\hat{D}_2 &= L_2(x_4 - \chi_4) \\ \dot{\chi}_4 &= \hat{\Gamma}_2^T\phi_2 + b_2u_2 + \hat{D}_2 - L_2^{-1}\omega_4\end{aligned} \tag{53}$$

in which L_2 is a positive real constant. So,

$$\dot{\hat{D}}_2 = L_2(\dot{x}_4 - \dot{\chi}_4) = L_2\left(\tilde{\Gamma}_2^T\phi_2 + \tilde{D}_2\right) + \omega_4 \tag{54}$$

Considering the adaptation law,

$$\dot{\hat{\Gamma}}_2 = \gamma_2\left(\omega_4\phi_2 - \delta_2\hat{\Gamma}_2\right) \tag{55}$$

where $\delta_2 > 0$ and the following inequalities that obtained by Young inequality lemma,

$$\begin{aligned}\tilde{D}_2\dot{D}_2 &\le \frac{1}{2}\tilde{D}_2^2 + \frac{1}{2}\zeta_2^2 \\ -\tilde{D}_2\tilde{\Gamma}_2^T\phi_2 &\le \frac{1}{2}\omega_2\tilde{D}_2^2\eta_2^2 + \frac{1}{2\omega_2}\tilde{\Gamma}_2^T\tilde{\Gamma}_2 \\ \tilde{\Gamma}_2^T\hat{\Gamma}_2 &\le -\frac{1}{2}\tilde{\Gamma}_2^T\tilde{\Gamma}_2 + \frac{1}{2}\|\Gamma_2^*\|^2\end{aligned} \tag{56}$$

in which $\omega_2 > 0$, Then, we have from (52),

$$\begin{aligned}\dot{V}_4 \le\ & -k_1\omega_1^2 - k_2\omega_2^2 - k_3\omega_3^2 - k_4\omega_4^2 \\ & - \left(\frac{\delta_1}{2} - \frac{L_1}{2\omega_1}\right)\tilde{\Gamma}_1^T\tilde{\Gamma}_1 \\ & - \left(L_1 - \frac{L_1\omega_1}{2}\eta_1^2 - \frac{1}{2}\right)\tilde{D}_1^2 \\ & + \left(\frac{\delta_1}{2}\|\Gamma_1^*\|^2 + \frac{1}{2}\zeta_1^2\right) - \left(\frac{\delta_2}{2} - \frac{L_1}{2\omega_2}\right)\tilde{\Gamma}_2^T\tilde{\Gamma}_2 \\ & - \left(L_2 - \frac{L_2\omega_2}{2}\eta_2^2 - \frac{1}{2}\right)\tilde{D}_2^2 \\ & + \left(\frac{\delta_2}{2}\|\Gamma_2^*\|^2 + \frac{1}{2}\zeta_2^2\right)\end{aligned} \tag{57}$$

Expressing equation (57) as $\dot{V}_4 \le -AV_4 + B$, where $A = \min\{k_i, \bar{\gamma}_j, \bar{D}_j\}$, $i \in \{1, \dots, 4\}$, $j \in \{1, 2\}$, and $B = \left(\frac{\delta_1}{2}\|\Gamma_1^*\|^2 + \frac{1}{2}\zeta_1^2 + \frac{\delta_2}{2}\|\Gamma_2^*\|^2 + \frac{1}{2}\zeta_2^2\right)$, it is evident that the overall system (25)-(28) exhibits uniformly ultimate boundedness (UUB) stability, ensuring that the signals involved in V_4 remain bounded.

For a clearer understanding of the proposed approach, a block diagram illustrating the structure of the model-free control scheme is provided in Fig. 3.

Simulation Results

The efficacy of the suggested technique is evaluated by applying it to a model with parameters outlined in [3] and [6] (see Table 2) and compares with sliding mode control and backstepping sliding mode. While various types of uncertainties, including motor specs, mass imbalance, friction torque, and wind disturbance, are considered, simulation conditions for all three control methods are identical.

This ensures that the noise and disturbances applied to the system in the simulation of the proposed method exactly match those applied during the simulation of the other two methods.

In typical scenarios, the load is often not centered at the gimbals' rotation center, leading to mass imbalance torque [40]. Additionally, bearing friction introduces a nonlinear torque acting as a disturbance. To simulate the influence of these disturbances, we consider the following torque expression,

$$T_{dL} = 1.7(rnd - 0.5)(\sin(\omega t) + \sin(2\omega t)), \tag{58}$$

where $L \in \{p, a\}$ represents pitch or yaw, respectively. Furthermore, to explore the nonlinear effects of gearing friction and other disturbances on the electric motors' torque, we propose,

$$T_{dm} = 0.04(\sin(\omega t) + \sin(2\omega t)) \tag{59}$$

Moreover, fluctuations in the gimbals' moment of inertia are set to be 20% of the nominal moment value. Thus, J_p and J_a can be represented as,

$$J_L = J_L^{nominal}\big(1 + 0.4\,(rnd - 0.5)\big), \qquad (60)$$

where $L \in \{p, a\}$. Simultaneously, random attitude perturbations of the helicopter's stationary base plate caused by wind disturbances are represented as,

$$\omega_{nb\tau}^{b}(t) = 0.6\,(rnd - 0.5), \qquad \tau \in \{x, y, z\} \qquad (61)$$

In the first scenario, with both the desired and initial attitude angles set to zero, Fig. 4 illustrates the attitude angles of pitch and yaw gimbals under the influence of the three control techniques.

Notably, the proposed control method exhibits significantly lesser deviation from the desired angles compared to both the backstepping control method and the backstepping sliding mode control method for both gimbals. This superiority is further evidenced by the mean squared errors presented in Table 3.

Table 3: Nominal values for the parameters of model

Parameter	Nominal Value	Unit
N	50	
J_m	2.7×10^{-4}	$Kg.m^2$
K_t	0.143	Nm/Amp
K_e	0.143	$V\,sec/rad$
R_m	7.56	Ω
$[J_{ax}, J_{ay}, J_{az}]^T$	$[0.540, 0.475, 0.162]^T$	$Kg.m^2$
$[J_{px}, J_{py}, J_{pz}]^T$	$[0.460, 0.267, 0.200]^T$	$Kg.m^2$
$[\omega_{nbx}^b, \omega_{nby}^b, \omega_{nbz}^b]^T$	$[0, 0, 0]^T$	rad/sec

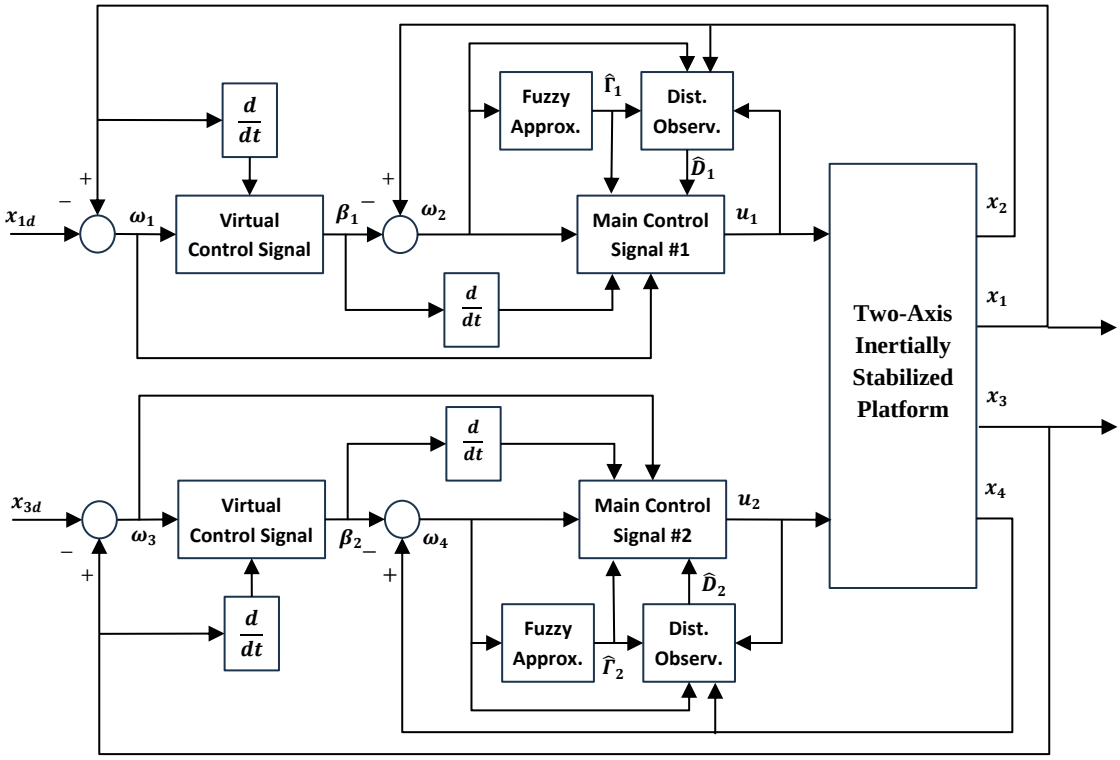

Fig. 3: Block Diagram of the proposed model-free control scheme for two-axis ISPs.

Table 2: Quantitative comparison of steady-state response in different scenarios for the evaluated control approaches

		Attitude angle of Pitch gimbal (deg.)			Attitude angle of Yaw gimbal (deg.)		
Scenario	**Approach**	$\max(\lvert e\rvert)$	$mse(e)$	$std(e)$	$\max(\lvert e\rvert)$	$mse(e)$	$std(e)$
	Backstepping	0.1535	0.0026	0.0507	0.1340	0.0015	0.0390
First	Backstepping SMC	0.0807	0.0004	0.0195	0.0759	0.0003	0.0175
	Proposed Method	0.0404	0.0001	0.0118	0.0474	0.0002	0.0136
	Backstepping	14.2217	5.3999	2.2386	11.2344	3.0565	1.6932
Second	Backstepping SMC	10.2482	1.5565	1.2276	10.1431	1.2727	1.1060
	Proposed Method	9.9973	0.4145	0.6341	10.0034	0.4096	0.6303

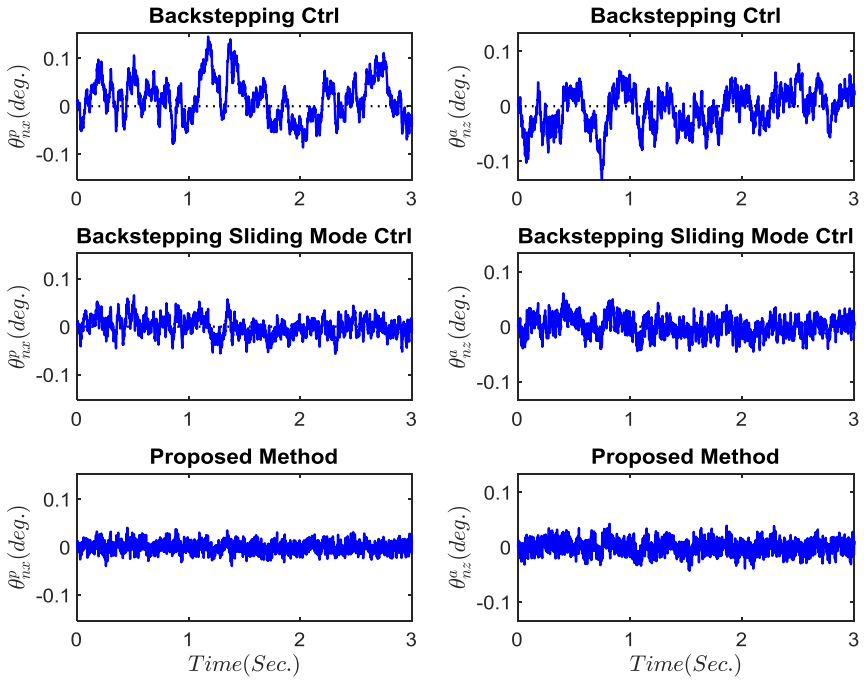

Fig. 4: Comparison of the steady-state response for both pitch and yaw gimbals in different control methods.

Although the proposed method performs best, however, the better performance of the backstepping sliding mode control compared to the pure backstepping technique is not far from expected because the sliding mode method is insensitive to parameter variations and external disturbances [6].

In the second scenario, a step of 10 degrees is introduced to the attitude angles of the yaw and pitch gimbals to assess the dynamic response characteristics of the control methods. Simulation results pertaining to this scenario are presented in Fig. 5 and Table 3, where once again, the proposed method outperforms the others. In terms of dynamic response, the proposed method settles the pitch gimbal in 0.1953 seconds, which is significantly faster than the pure backstepping control (0.4497 seconds) and the backstepping sliding mode method (0.4595 seconds). Similarly, the overshoot in the proposed method is 76% and 36% less than in pure backstepping and backstepping sliding mode control, respectively. Further details regarding the dynamic response characteristics of the investigated methods for both yaw and pitch gimbals are summarized in Table 4.

Besides, to evaluate the control effort exerted by the proposed method and assess its effectiveness, we compare the control effort u_2 for the Yaw gimbal in Fig. 6. It is evident that, generally, there is not a significant difference in control effort required. However, at the moment of angle change (1.5 seconds), the control effort in SMC-based methods is notably lower compared to the pure backstepping approach. Furthermore, the performance of the proposed method in terms of lamped disturbance tracking is depicted in Fig. 7, demonstrating the effective capability of the proposed approach to simultaneously estimate disturbances and uncertainties present in the system.

Table 4: Quantitative comparison of the transient response caused by using the control methods in pitch and yaw gimbals

Approach	Settling Time (Sec.)	Peak (deg.)	Overshoot (%)
Values for pitch gimbal evaluation			
Backstepping	0.4497	24.2217	142.2168
Backstepping SMC	0.4595	20.2482	102.4815
Proposed Method	0.1953	16.6126	66.1255
Values for yaw gimbal evaluation			
Backstepping	0.4438	21.2344	112.3436
Backstepping SMC	0.4533	20.1431	101.4314
Proposed Method	0.1875	16.3361	63.3610

Since fuzzy systems and disturbance observers are sharing information with each other, one cannot precisely determine whether fuzzy estimator can approximate d_2. Hence, the aim of the proposed controller is achieved in view of the estimation task, if the estimation can track the lumped uncertainty with high precision. This job is confirmed by Fig. 7.

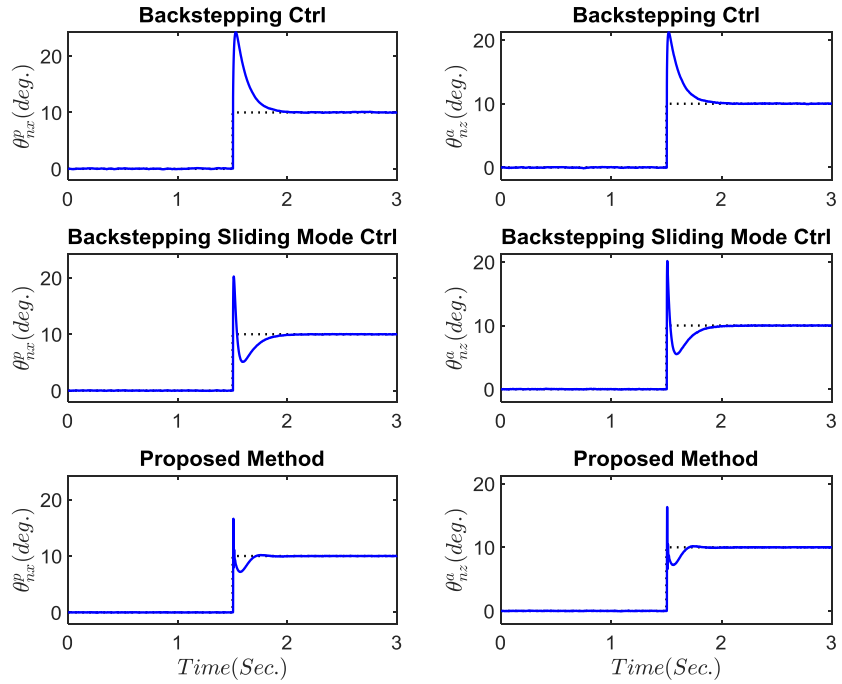

Fig. 5: Comparing transient response to a 10-degree step change in pitch and yaw gimbals attitudes.

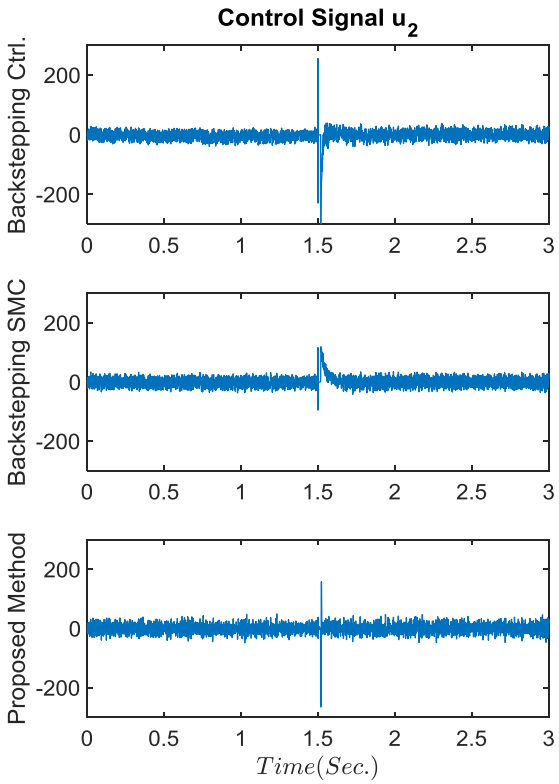

Fig. 6: Comparison of control signals for yaw gimbal in the second scenario.

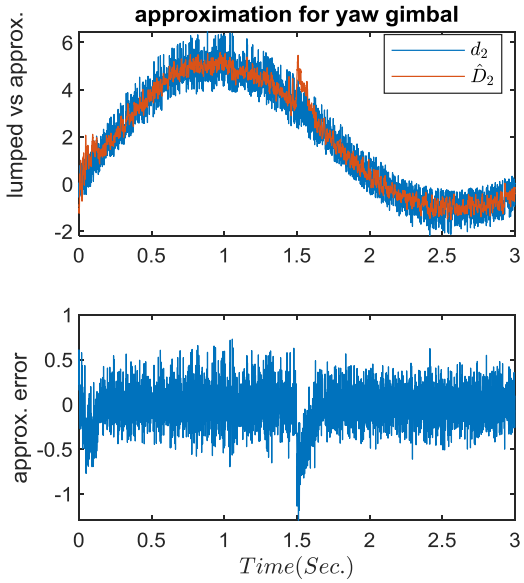

Fig. 7: Performance of the disturbance estimator for lumped disturbances of yaw gimbal in Scenario 2.

Conclusion

In order to enhance the control performance of the ISP system, a disturbance observer-based adaptive fuzzy backstepping controller is developed in this paper. Integrated with a model-free disturbance observer, it ensures high-performance control in uncertain environments. In addition, the stabilization control with high accuracy is also provided in the presence of various uncertainties. The recursive Lyapunov-based analysis confirms the uniformly ultimate boundedness stability of the overall system.Different simulations and comparisons with two relevant control techniques, namely the backstepping control and the backstepping sliding mode control, demonstrate the proposed controller's superiority in the perspective of the transient

response and the steady-state response. Inspired by the current study, we will present an adaptive constrained model-free fault-tolerant control scheme for the ISP system in the future.

Author Contributions

In the current study, the roles of each individual were as follows: M. Ghalehnoie, J. Keighobadi, and A. Azhdari conducted the experimental design. Software development and simulations were carried out by M. Ghalehnoie and A. Azhdari. Following this phase, M. Ghalehnoie collected and analyzed the data. The initial drafting of the manuscript was undertaken collaboratively by M. Ghalehnoie, A. Azhdari, and J. Keighobadi. Subsequently, M. Ghalehnoie and J. Keighobadi provided critical revision of the manuscript. Additionally, supervision of the research execution was provided by M. Ghalehnoie.

Acknowledgment

The authors would like to express their sincere gratitude to the reviewers and editors of JECEI for their constructive comments and valuable suggestions, which have significantly enhanced the quality of this article. Additionally, the authors are thankful to the editorial board for their support and professional handling of the manuscript throughout the review process.

Conflict of Interest

The authors declare no potential conflict of interest regarding the publication of this work. In addition, the ethical issues including plagiarism, informed consent, misconduct, data fabrication and, or falsification, double publication and, or submission, and redundancy have been completely witnessed by the authors.

Abbreviations

DOB	Disturbance Observer
ISMC	Integral Sliding Mode Control
ISP	Inertially Stabilized Platform
PID	Proportional Integral Derivative
SMC	Sliding Mode Control

References

[1] J. M. Hilkert, "Inertially stabilized platform technology Concepts and principles," IEEE Control Syst, 28(1): 26-46, 2008.

[2] M. K. Masten, "Inertially stabilized platforms for optical imaging systems," IEEE Control Syst, 28(1): 47-64, 2008.

[3] X. Lei, Y. Zou, F. Dong, "A composite control method based on the adaptive RBFNN feedback control and the ESO for two-axis inertially stabilized platforms," ISA Trans, 59: 424-433, 2015.

[4] J. Mao, S. Li, Q. Li, J. Yang, "Design and implementation of continuous finite-time sliding mode control for 2-DOF inertially stabilized platform subject to multiple disturbances," ISA Trans, 84: 214-224, 2019.

[5] J. Mao, J. Yang, X. Liu, S. Li, Q. Li, "Modeling and robust continuous TSM control for an inertially stabilized platform with couplings," IEEE Trans. Control Syst. Technol., 28(6): 2548-2555, 2020.

[6] F. Dong, X. Lei, W. Chou, "A dynamic model and control method for a Two-Axis inertially stabilized platform," IEEE Trans. Ind. Electron., 64(1): 432-439, 2017.

[7] X. Zhou, H. Zhang, R. Yu, "Decoupling control for two-axis inertially stabilized platform based on an inverse system and internal model control," Mechatronics, 24(8): 1203-1213, 2014.

[8] Q. Mu, G. Liu, X. Lei, "A RBFNN-Based adaptive disturbance compensation approach applied to magnetic suspension inertially stabilized platform," Math. Probl. Eng., 2014: 1-9, 2014.

[9] X. Zhou, G. Gong, J. Li, H. Zhang, R. Yu, "Decoupling control for a three-axis inertially stabilized platform used for aerial remote sensing," Trans. Inst. Meas. Control, 37(9): 1135-1145, 2015.

[10] S. Liu, H. Che, L. Sun, "Research on stabilizing and tracking control system of tracking and sighting pod," J. Control Theory Appl., 10(1): 107-112, 2012.

[11] F. Liu, H. Wang, "Fuzzy PID tracking controller for two-axis airborne optoelectronic stabilized platform," Int. J. Innovative Computi. Inf. Control, 13(4): 1307-1322, 2017.

[12] N. Ghaeminezhad, W. Daobo, F. Farooq, "Stabilizing a gimbal platform using self-tuning fuzzy PID controller," Int. J. Comput. Appl., 93(16): 13-19, 2014.

[13] Q. Guo, G. Liu, B. Xiang, T. Wen, H. Liu, "Robust control of magnetically suspended gimbals in inertial stabilized platform with wide load range," Mechatronics, 39: 127-135, 2016.

[14] S. Hong, K. D. Cho, C. H. Park, W. S. Kang, "Trajectory generation and H∞ robust control for inertially stabilized system," in Proc. 2011 IEEE/ASME International Conference on Advanced Intelligent Mechatronics (AIM): 695-700, 2011.

[15] A. Toloei, H. Asgari, "Quaternion-based finite-time sliding mode controller design for attitude tracking of a rigid spacecraft during high-thrust orbital maneuver in the presence of disturbance torques," Int. J. Eng., 32(3): 430-437, 2019.

[16] T. Wen, B. Xiang, W. Wong, "Coupling analysis and cross-feedback control of three-axis inertially stabilized platform with an active magnetic bearing system," Shock Vibr., 2020: 1-17, 2020.

[17] X. Zhou, Y. Shi, L. Li, R. Yu, L. Zhao, "A high precision compound control scheme based on non-singular terminal sliding mode and extended state observer for an aerial inertially stabilized platform," Int. J. Control Autom. Syst., 18(6): 1498–1509, 2020.

[18] H.-C. Park, S. Chakir, Y. B. Kim, T. Huynh, "a nonlinear backstepping controller design for high-precision tracking applications with input-delay gimbal systems," J. Mar. Sci. Eng., 9(5): 530, 2021.

[19] J. Deng, W. Xue, X. Zhou, Y. Mao, "On disturbance rejection control for inertial stabilization of long-distance laser positioning with movable platform," Meas. Control, 53(7–8): 1203-1217, 2020.

[20] Y. Wang, H. Lei, J. Ye, X. Bu, "Backstepping sliding mode control for radar seeker servo system considering guidance and control system," Sensors, 18(9): 2927, 2018.

[21] R. Yazdanpanah, J. Soltani, "Robust backstepping control of induction motor drives using artificial neural networks and sliding mode flux observers," Int. J. Eng., 20(3): 221-232, 2007.

[22] M. M. Zohrei, A. Roosta, "Constrained adaptive backstepping sliding mode control for inertial stable platform," Iran. J. Sci. Technol. Trans. Electr. Eng., 46(3): 753-764, 2022.

[23] M. M. Zohrei, A. Roosta, B. Safarinejadian, "Robust backstepping control based on neural network stochastic constrained for three axes inertial stable platform," J. Aerosp. Eng., 35(1): 2022.

[24] I. S. Azzam, A. G. Wassal, S. A. Maged, "Line of sight control strategies for inertial stabilization platforms: comparative study," in Proc. 2021 16th International Conference on Computer Engineering and Systems (ICCES): 1-7, 2021.

[25] M. F. Reis, J. C. Monteiro, R. R. Costa, A. C. Leite, "Super-twisting control with quaternion feedback for a 3-DoF inertial stabilization platform," in Proc. 2018 IEEE Conference on Decision and Control (CDC): 2193-2198, 2018.

[26] S. Dey, T. K. Sunil Kumar, S. Ashok, S. K. Shome, "Robust cascade control strategy for trajectory tracking to decouple disturbances using 3-degree-of-freedom inertial stabilized platform and its experimental validation," Trans. Inst. Meas. Control, 2023.

[27] H. Khodadadi, M. R. J. Motlagh, M. Gorji, "Robust control and modeling a 2-DOF Inertial Stabilized Platform," in Proc. International Conference on Electrical, Control and Computer Engineering 2011 (InECCE): 223-228, 2011.

[28] A. Assoud, A. V. Polynkov, "Improving the stabilization accuracy of a platform using active disturbance rejection control and field-oriented control," in AIP Conference Proceeding, 2549(1), 2023.

[29] F. Wang, R. Wang, E. Liu, W. Zhang, "Stabilization control mothed for two-axis inertially stabilized platform based on active disturbance rejection control with noise reduction disturbance observer," IEEE Access, 7: 99521-99529, 2019.

[30] S. Asgari, M. B. Menhaj, A. A. Suratgar, M. G. Kazemi, "A disturbance observer based fuzzy feedforward proportional integral load frequency control of microgrids," Int. J. Eng., 34(7): 1694-1702, 2021.

[31] X. Liu, J. Mao, J. Yang, S. Li, K. Yang, "Robust predictive visual servoing control for an inertially stabilized platform with uncertain kinematics," ISA Trans, 114: 347-358, 2021.

[32] D. Tian, M. Wang, F. Wang, R. Xu, "Adaptive sliding-mode-assisted disturbance observer-based decoupling control for inertially stabilized platforms with a spherical mechanism," IET Control Theory Appl., 16(12): 1194-1207, 2022.

[33] A. Kodhanda, J. P. Kolhe, M. M. Kuber, V. V. Parlikar, "Uncertainty and disturbance estimation based control of three-axis stabilized platform," Int. J. Latest Trends Eng. Technol., 3(3): 289-297, 2014.

[34] Z. Ding, F. Zhao, Y. Lang, Z. Jiang, J. Zhu, "Anti-disturbance neural-sliding mode control for inertially stabilized platform with actuator saturation," IEEE Access, 7: 92220-92231, 2019.

[35] X. Yan, M. Chen, G. Feng, Q. Wu, S. Shao, "Fuzzy robust constrained control for nonlinear systems with input saturation and external disturbances," IEEE Trans. Fuzzy Syst., 29(2): 345-356, 2021.

[36] B. Xu, "Composite learning control of flexible-link manipulator using NN and DOB," IEEE Trans Syst. Man Cybern. Syst., 48(11): 1979-1985, 2018.

[37] M. M. Zohrei, H. R. Javanmardi, "Nonlinear observer-based control design for a three-axis inertial stabilized platform," J. Appl. Res. Electr. Eng., 2(2): 158-172, 2024.

[38] L. Wang, X. Li, Y. Liu, D. Mao, B. Zhang, "High-precision control of aviation photoelectric-stabilized platform using extended state observer-based kalman filter," Sensors, 23(22): 9204, 2023.

[39] H. Gorjizadeh, M. Ghalehnoie, S. Negahban, A. Nikoofard, "Fuzzy controller design for constant bottomhole pressure drilling under operational/physical constraints," J. Pet. Sci. Eng., 212: 110335, 2022.

[40] N. H. Giap, J. H. Shin, W. H. Kim, "Robust adaptive neural network control for XY table," Intell. Control Autom., 04(03): 293-300, 2013.

Biographies

Mohsen Ghalehnoie was born in Shahrood, Iran, in 1982, and holds Bachelor's, Master's, and Doctoral degrees in Control Engineering. He earned his B.Sc. and M.Sc. degrees from Iran University of Science and Technology and the University of Tehran in 2005 and 2008, respectively. Additionally, he received his Ph.D. from Ferdowsi University of Mashhad in 2018. Currently, he serves as an assistant Professor of Control Engineering at Shahrood University of Technology, Shahrood, Iran. His work focuses on control systems theory, optimization, fuzzy control, data fusion, and expert systems, especially for hybrid switched systems and industrial processes.

- Email: ghalehnoie@shahroodut.ac.ir
- ORCID: 0000-0001-8012-262X
- Web of Science Researcher ID: AFL-9790-2022
- Scopus Author ID: 27367994200
- Homepage: https://shahroodut.ac.ir/fa/as/?id=S917

Ali Azhdari was born in Shiraz, Iran, in 1995. He received his Bachelor's degree in Control Electrical Engineering from Fasa University in 2018 and his Master's degree in the same field from Shahrood University of Technology in 2021. His current research focuses on Buck and Multi-level converters. He is particularly interested in Classic control methodologies such as back-stepping control, Super twisting algorithms, Sliding Mode Control, and adaptive control. Additionally, he has expertise in fuzzy controllers and optimization methods.

- Email: aliazhdari.pro@gmail.com
- ORCID: 0000-0002-9779-1683
- Web of Science Researcher ID: JHT-1749-2023
- Scopus Author ID: NA
- Homepage: https://www.linkedin.com/in/ali-azhdari-2ab243180

Javad Keighobadi his B.Sc., M.Sc. and Ph.D. degrees from Shahrood University of Technology, in 2012, 2014 and 2020, respectively. Currently, He is an assistant professor with the Faculty of Electrical Engineering at Shahrood University of Technology. His research interests include Nonlinear Control, Fault-tolerant Systems, Robotics and Intelligent Control.

- Email: javad_keighobadi@shahroodut.ac.ir
- ORCID: 0000-0001-6474-5499
- Web of Science Researcher ID: KYQ-0669-2024
- Scopus Author ID: 57211945901
- Homepage: https://shahroodut.ac.ir/fa/as/index.php?id=S1148

How to cite this paper:
M. Ghalehnoie, A. Azhdari, J. Keighobadi, ” Robust fuzzy control of uncertain two-axis inertially stabilized platforms using a disturbance observer: A backstepping-based adaptive control approach,” J. Electr. Comput. Eng. Innovations, 13(1): 13-26, 2025.

DOI: 10.22061/jecei.2024.10886.746

URL: https://jecei.sru.ac.ir/article_2171.html